

Supporting Information A:

Elucidating the spatial distribution of organic contaminants and their biotransformation products in amphipod tissue by MALDI- and DESI-MS-imaging

Johannes Raths^{1,2}, Fernanda E. Pinto³, Christian Janfelt³, Juliane Hollender^{1,2*}

¹Department of Environmental Chemistry, Swiss Federal Institute of Aquatic Science and Technology - Eawag, Dübendorf, Switzerland

²Institute of Biogeochemistry and Pollutant Dynamics, ETH Zürich, Zürich, Switzerland

³Department of Pharmacy, University of Copenhagen, Copenhagen, Denmark

Corresponding author:

juliane.hollender@eawag.ch

Contents

SI A1: Test compounds	1
SI A2: LC-HRMS/MS analysis.....	2
Online-SPE LC-HRMS/MS settings	2
Analytical quality parameters	4
Identified biotransformation products	5
SI A3: Biotransformation pathways.....	7
SI A4: Histological staining.....	9
SI A5: Medium concentrations.....	10
SI A6: Bioconcentration potential across different studies.....	10
SI A7: Tissue concentrations.....	11
SI A8: Biotransformation ratio across different compartments.....	12
SI A9: MSI - Supplementary images and replicates.....	13
SI A10: MSI - Mass interferences.....	18
References.....	19

SI A1: Test compounds

A summary of the selected test compounds, which were used for the exposure mixture, is presented in Table S1.

Table S1: Physico-chemical properties and modes of action of the selected test-compounds derived from <https://pubchem.ncbi.nlm.nih.gov/>. Log D_{ow} is the Log K_{ow} adjusted to the speciation at the pH of interest (pH 7.9). The log D_{ow} was derived from <https://chemicalize.com/> using a QSAR analysis that calculates the octanol-water partitioning coefficients at pH 7.9. Acute LC₅₀ reported for gammarids and if not available for daphnids (D).

Compound (shortcut)	CAS	Molecular formula	Molecular weight	Class	MoA (Use)	log K _{ow}	log D _{ow}	pKa	Charge at pH 7.9	Acute LC ₅₀ [mg L ⁻¹] (reference)
Carbamazepine (CMZ)	298-46-4	C ₁₅ H ₁₂ N ₂ O	236.3	Pharmaceutical	Voltage-gated Sodium channels (anti-epileptic)	2.3	2.3	n.d.	neutral	NOEC > 1 (chronic) (Heye et al., 2019)
Citalopram (CIT)	59729-33-8	C ₂₀ H ₂₁ FN ₂ O	324.4	Pharmaceutical	Sel. serotonin reuptake inhibitor (Anti-depressant)	3.5	1.9	9.8	cation	20 (D) (Christensen et al., 2007)
Cyprodinil (CY)	121552-61-2	C ₁₄ H ₁₅ N ₃	225.3	Fungicide	Inhibits protein synthesis	4.0	4.0	4.4	neutral	3.0 (Ashauer et al., 2011)
Efavirenz (EF)	154598-52-4	C ₁₄ H ₉ ClF ₃ NO ₂	315.7	Pharmaceutical	Antiretroviral, reverse transcriptase inhibitor	4.6	4.6	10.2	neutral	> 1.0 (D) (Mahaye and Musee, 2022)
Fluopyram (FLU)	658066-35-4	C ₁₆ H ₁₁ ClF ₆ N ₂ O	396.7	Fungicide	Succinate dehydrogenase inhibitor	3.3	3.3	n.d.	neutral	2.3 (D) (Li et al., 2021)
Terbutryn (TER)	886-50-0	C ₁₀ H ₁₉ N ₅ S	241.4	Herbicide	PSII inhibitor	3.7	3.7	4.3	neutral	> 1.5 (Richter and Nagel, 2007)

SI A2: LC-HRMS/MS analysis

Analytical settings and quality parameters are presented in Table S2 to Table S7.

Online-SPE LC-HRMS/MS settings

To prepare the online-SPE column, 8-9 mg of Oasis HLB (15 µm particle size, Waters) were added to an empty stainless steel SPE cartridge (20 mm x 2.1 mm, BGB Analytik AG). Next, the cartridge was filled with about 8-9 mg of a mix of anion exchanger Strata X-AW, cation exchanger Strata X-CW (both ion exchangers: 30 µm, Phenomenex, UK) and Env+ (70 µm, Biotage, Sweden) in a ratio of 1:1:1.5 (X-AW : X-CW : Env+).

Table S2: Schedule of the online-SPE.

Time [min]	Acetonitrile [µL min ⁻¹]	Ammonium acetate solution (2 mM) [µL min ⁻¹]	SPE step
0		200	Elution of the sample from the cartridge (with elution pump) and washing of the loop.
0.1	4000		
1.1	4000		
1.2		4000	
6.7		4000	
6.8		400	
7.3		400	
7.4	400		Loading of the new sample into the loop and conditioning of the cartridge.
12.5	400		
12.6		400	
18.4		400	
18.5		1270	Enrichment of the new sample.
32.1		1270	
34.5		1270	
34.7		1270	
35		200	

Table S3: Schedule of the liquid chromatography. Water and methanol were both acidified with 0.1% (vol.) formic acid. Chromatographic separation was performed with a reversed-phase column (Atlantis T3 C18 column, 5 µm, 3x150 mm, Waters, Batch No 0151351351)

Time [min]	H ₂ O [µL min ⁻¹]	MeOH [µL min ⁻¹]
0.0	0.260	0.040
5.0	0.260	0.040
20.0	0.015	0.285
29.0	0.015	0.285
29.5	0.260	0.040
35.0	0.260	0.040

Table S4: Source parameters used for HRMS/MS measurement with the QExactive Plus mass spectrometer.
 *External mass calibration with an in-house prepared amino acid solution (11 amino acids with m/z between 116 and 997) in positive and negative ionization mode.

Parameter	Value
Sheath gas (nitrogen) flow rate	40 L min ⁻¹
Auxiliary gas (nitrogen) flow rate	15 L min ⁻¹
Capillary temperature	320 °C
S-lens RF level	50
Mass calibration	External*
Spray voltage	4 kV (positive ionisation mode)

Table S5: MS parameters used for HRMS/MS measurement with the QExactive Plus mass spectrometer.

Parameter	Value
Resolution	70k
Scan range	150-2000 m/z
Polarity	Positive
Resolution MS2	30k

Analytical quality parameters

Table S6: Analytical quality parameters of the quantified parent compounds calculated according to Huntscha et al. (2012). ISTD = internal standard. All ISTDs were deuterated analogues of the target analytes. Concentrations can be transformed from metric to molar concentrations by using the molecular weight provided in Table S1. The BTP shortcuts are comprised of the parent name, M = metabolite and their m/z values of $[M+H]^+$. Terbutryn BTPs were quantified based on the calibration and recovery of TER_M214 (Irgarol-descyclopropyl), due to more similar retention times and higher ionization efficiencies than the parent compound as applied earlier (Kosfeld et al., 2020; Rath et al., 2023).

	Matrix factor						LOQ [$\mu\text{g kg}^{-1}$] (for medium $\mu\text{g L}^{-1}$)						
Compound (shortcut)	Medium	Whole body	Gill	Intestinal system	Cephalon	Remaining tissue	Medium	Whole body	Gill	Intestinal system	Cephalon	Remaining tissue	Quantification (isotope label ISTD)
Carbamazepine (CMZ)	0.81	0.81	1.23	1.09	0.98	0.67	0.006	0.11	37	1.2	0.53	0.12	Reference standard and ISTD (d8)
Citalopram (CIT)	0.97	0.73	1.32	1.22	0.95	0.69	0.005	0.13	34	1.1	0.55	0.12	Reference standard and ISTD (d6)
Cyprodinil (CY)	1.07	0.75	1.13	1.08	0.89	0.61	0.023	0.61	200	6.2	3.0	0.68	Reference standard and ISTD (d5)
Efavirenz (EF)	0.89	0.58	1.09	0.94	0.81	0.45	0.028	0.79	210	7.20	3.2	0.92	Reference standard and ISTD (d5)
Fluopyram (FLU)	1.02	0.57	1.18	1.09	0.93	0.46	0.012	0.40	97	3.10	1.4	0.45	Reference standard and ISTD (d4)
Terbutryn (TER)	0.83	0.64	1.10	0.92	0.81	0.53	0.015	0.36	100	3.7	1.6	0.39	Reference standard and ISTD (d5)
	Matrix factor						LOQ [$\mu\text{g kg}^{-1}$] (for medium $\mu\text{g L}^{-1}$)						
BTP shortcut (full name)	Medium	Whole body	Gill	Intestinal system	Cephalon	Remaining tissue	Medium	Whole body	Gill	Intestinal system	Cephalon	Remaining tissue	(Semi-)Quantification
CMZ_M253 (CMZ-10-11-epoxide)	0.81	0.81	1.23	1.09	0.98	0.67	0.006	0.11	37	1.24	0.5	0.12	Reference standard and ISTD of parent
CIT_M297 (CIT-didesmethyl)	0.97	0.73	1.32	1.22	0.95	0.69	2.6	63	17187	552	275	60	Reference standard and ISTD of parent
CIT_M311 (CIT N-desmethyl)	0.97	0.73	1.32	1.22	0.95	0.69	0.026	0.63	172	5.52	2.8	0.60	Reference standard and ISTD of parent
CY_M242b	1.07	0.75	1.13	1.08	0.89	0.61	0.023	0.61	201	6.23	2.95	0.68	Based on CY_M242a (CGA 304075) and parent ISTD
TER_M214 (Irgarol-descyclopropyl)	0.83	0.64	1.10	0.92	0.81	0.53	0.003	0.07	21	0.73	0.32	0.08	Reference standard and ISTD of parent
TER_M258a	0.83	0.64	1.10	0.92	0.81	0.53	0.003	0.07	21	0.73	0.32	0.08	Based on TER_M214 (Irgarol-descyclopropyl)
TER_M315a and b	0.83	0.64	1.10	0.92	0.81	0.53	0.003	0.07	21	0.73	0.32	0.08	Based on TER_M214 (Irgarol-descyclopropyl)

Identified biotransformation products

Table S7: Inclusion list and detection of BTPs. Green shading: parent compound with reference standard in the calibration curve and matching ISTD, yellow shading: BTP with reference standard in the calibration curve confidence (level 1; Schymanski et al., 2014); red shading: BTP with no reference standard but diagnostic MS/MS fragments available (level 2a). Mode = ionisation mode. G = *G. pulex*; Cal = calibration; Q = quantified. 1 (blue) = compound detected in at least one sample; 0 (pink) = compound not detected; 0.5 (orange) = compound detected (i.e. in calibration) but should not be present (potentially formed from parent compound or impurity). Such compounds were excluded from quantification and further analysis. y = yes (quantified); n = no (not quantified). BTPs with little intensities (< 5% parent) were not quantified. References for detection of the BTPs in environmental matrices can be used for further details on the BTP identification such as MS/MS spectra. Some BTPs were added to the list, because reference standards were available.

Compound	Molecular Formula	Mode	[M+H] ⁺	G	Cal	Q	Reference
Carbamazepine	C15H12N2O	pos	237.1022	1	1	y	
CMZ_dihydro	C15H14N2O1	pos	239.1179	0	1	n	Standard available
CMZ_dihydro-dihydroxy	C15H14N2O3	pos	271.1077	0	1	n	Standard available
CMZ_Oxcarbazepine	C15H12N2O2	pos	253.0972	0	1	n	Standard available
CMZ_Iminostilben	C14H11N1	pos	194.0964	0	1	n	Standard available
CMZ_epoxide	C15H12N2O2	pos	253.0972	1	1	y	(Jeon and Hollender, 2019; Rath et al., 2023)
Citalopram	C20H21FN2O	pos	325.1711	1	1	y	
CIT N-desmethyl	C19H19FN2O	pos	311.1554	1	1	y	(Rath et al., 2023)
CIT N-oxide	C20H23N2O2F1	pos	341.1660	1	1	y	(Rath et al., 2023)
CIT didesmethyl	C20H21FN2O2	pos	297.1398	1	1	y	(Rath et al., 2023)
Cyprodinil	C18H17FN2O	pos	226.1339	1	1	y	
CY-TP CGA 249287	C8H11N3	pos	150.1026	1	1	n	(Kiefer et al., 2019)
CY_M378	C17H19N3O5S	pos	378.1118	0	0	n	(Sapp et al., 2004)
CY_M362	C17H19N3O4S	pos	362.1169	0	0	n	(Sapp et al., 2004)
CY_M242a (CY_CGA_304075)	C14H15N3O	pos	242.1288	1	1	n	(Rath et al., 2023; Sapp et al., 2004)
CY_M242b	C14H15N3O	pos	242.1288	1	0	y	(Rath et al., 2023; Sapp et al., 2004)
CY_M242 c, d, e	C14H15N3O	pos	242.1288	1	0	n	(Sapp et al., 2004)
CY_M345	C17H20N4O2S	pos	345.1380	0	0	n	(Sapp et al., 2004)
CY_M240	C14H13N3O	pos	240.1131	1	0	n	(Sapp et al., 2004)
CY_M151	C8H10N2O	pos	151.0866	0	0	n	(Sapp et al., 2004)
CY_M136	C7H9N3	pos	136.0869	0	0	n	(Sapp et al., 2004)
Efavirenz	C14H9ClF3NO2	pos	316.0347	1	1	1	
Efavirenz-Methyl	C15H11ClF3NO2	pos	330.0503	1			(Mutlib et al., 2000)
Efavirenz-OH	C14H9ClF3NO3	pos	332.0296	1			(Mutlib et al., 2000)
Fluopyram	C16H11ClF6N2O	pos	397.0537	1	1	y	
FLU_TMB (Fluopyram Benzamide)	C8H6F3NO	pos	190.0474	1	1	n	(Vargas-Pérez et al., 2020)
PCA (3-Chloro-5-(trifluoromethyl)picolinic acid) (or TPA, Wie 2016)	C7H3ClF3NO2	pos*	225.9877	0	1	n	(Vargas-Pérez et al., 2020)
FLU_TPAA (Fluopyram-PAA in Vargas)	C8H5ClF3NO2	pos	240.0034	0	0	n	(Vargas-Pérez et al., 2020)
FLU-7-OH /8-OH	C16H11ClF6N2O2	pos	413.0486	1	0	n	(Vargas-Pérez et al., 2020)

FLU_2,9-bis(trifluoromethyl)-6,7-dihydropyrido[2,3-e][2]benzazocin-8(5H)-one	C16H10F6N2O	pos	361.0770	0	0	n	(Vargas-Pérez et al., 2020)
FLU-OH	C16H9ClF6N2O2	pos	411.0329	0	0	n	(Vargas-Pérez et al., 2020)
FLU-OH-GA	C22H19ClF6N2O8	pos	589.0807	0	0	n	(Vargas-Pérez et al., 2020)
FLU-OH-glc	C22H21ClF6N2O7	pos	575.1014	0	0	n	(Vargas-Pérez et al., 2020)
FLU-OH-glc-MA	C25H23ClF6N2O10	pos	661.1018	0	0	n	(Vargas-Pérez et al., 2020)
FLU-OH-SA	C16H11ClF6N2O5S	pos	493.0054	0	0	n	(Vargas-Pérez et al., 2020)
FLU-olefin	C16H9ClF6N2O	pos	395.0381	0	0	n	(Vargas-Pérez et al., 2020)
FLU-pic	C7H5ClF3N	pos	196.0136	0	0	n	(Vargas-Pérez et al., 2020)
FLU-benzoic acid	C8H5F3O2	pos*	191.0314	0	0	n	(Vargas-Pérez et al., 2020)
FLU-methyl-sulfoxide	C8H6SNO3	pos*	197.0141	0	0	n	(Vargas-Pérez et al., 2020)
FLU_2,9-bis(trifluoromethyl)-6,7-dihydropyrido[2,3-e][2]benzazocin-8(5H)-one	C16H10F6N2O	pos*	361.0770	0	0	n	(Vargas-Pérez et al., 2020)
Terbutryn	C10H19N5S	pos	242.1434	1	1	y	
TER_lrgarol-descyclopropyl	C8H15N5S1	pos	214.1121	1	1	y	(Jeon et al., 2013; Rath et al., 2023)
TER_MTE258a	C10H20N5S	pos	258.1384	1	0	y	(Jeon et al., 2013; Rath et al., 2023)
TER_MTE258b	C10H20N5S	pos	258.1384	0.5	0.5	n	(Jeon et al., 2013; Rath et al., 2023)
TER_MTE272	C10H18O2N5S	pos	272.1174	1	0	n	(Jeon et al., 2013; Rath et al., 2023)
TER_MTE315a	C12H22N6O2S	pos	315.1602	1	0	y	(Jeon et al., 2013; Rath et al., 2023)
TER_MTE315b	C12H22N6O2S	pos	315.1602	1	0	y	(Jeon et al., 2013; Rath et al., 2023)
TER_MTE501	C19H33O6N8S	pos	501.2236	1	0	n	(Jeon et al., 2013; Rath et al., 2023)

*Better ionization efficiency expected in negative mode

SI A3: Biotransformation pathways

The biotransformation reactions of the quantified BTPs are summarized in Table S8. It is important to mention, that no non-target analysis of BTPs was performed. BTP analysis was based on a suspect screening from literature reports. Thus, this table does not claim completeness. However, the BTP list of terbutryn is based on an extensive screening by Jeon et al. (2013). Biotransformation pathways are illustrated in Figure S1 to Figure S4.

Table S8: Biotransformation product classification for the quantified BTPs. 1st = primary BTPs, 2nd = secondary BTPs. References for the biotransformation pathways are provided.

Parent	BTP	Classification	Pathway	Reference
Carbamazepine	CMZ_M253 (CMZ 10,11-epoxide)	1 st	Oxidation	(Jeon and Hollender, 2019), Figure S1
Citalopram	CIT_M311 (CIT N-desmethyl)	1 st	N-dealkylation	(Raths et al., 2023; Sangkuhl et al., 2011)
Citalopram	CIT_M297 (CIT didesmethyl)	2 nd	N-dealkylation	(Raths et al., 2023; Sangkuhl et al., 2011), Figure S2
Cyprodinil	CY_M242b	1 st	Hydroxylation at benzene group	(Raths et al., 2023), Figure S3
Terbutryn	TER_M214 (Irgarol-descyclopropyl)	1 st	Dealkylation	(Jeon et al., 2013), Figure S4
Terbutryn	TER_M258a	1 st	Hydroxylation at tert-butyl group	(Jeon et al., 2013), Figure S4
Terbutryn	TER_M315a	2 nd	Glutathione conjugation → carboxyl peptidase → glutamyl transpeptidase → rearrangement	(Jeon et al., 2013), Figure S4
Terbutryn	TER_M315b	2 nd	Glutathione conjugation → carboxyl peptidase → glutamyl transpeptidase → rearrangement	(Jeon et al., 2013), Figure S4

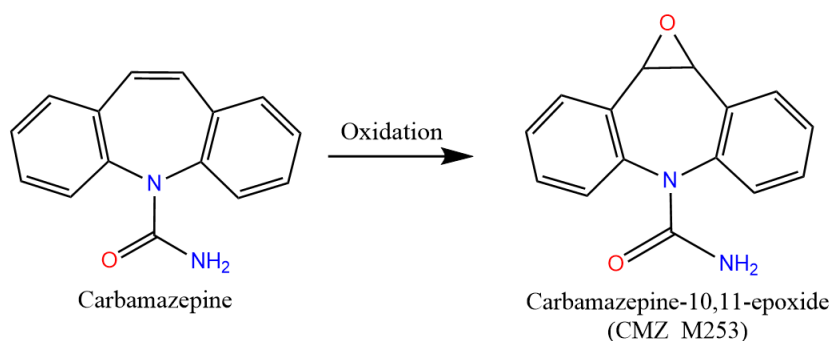


Figure S1: Biotransformation pathway of carbamazepine-10,11-epoxide (CMZ_M253) based on Jeon & Hollender (2019).

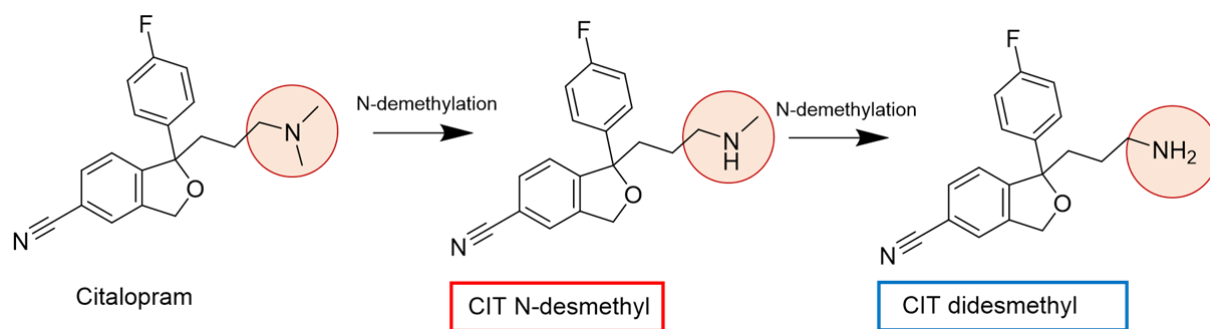


Figure S2: Biotransformation pathways of citalopram in *G. pulex*. Red = primary BTP, blue = secondary BTP. CIT = citalopram. Based on Rath et al. (2023).

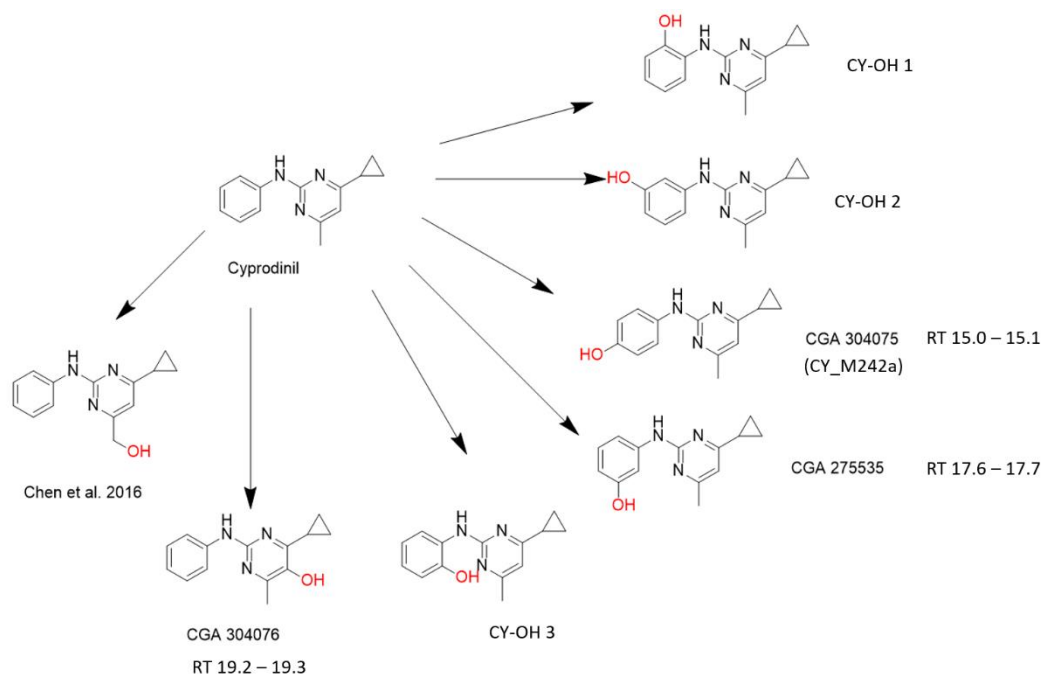


Figure S3: Overview of the possible hydroxylation BTPs of cyprodinil (= CY_M242). CY_M242b is one of the phenol BTPs (CY_OH 1 to 3). Adapted from Rath et al. (2023) further details on the identification are provided in the corresponding SI.

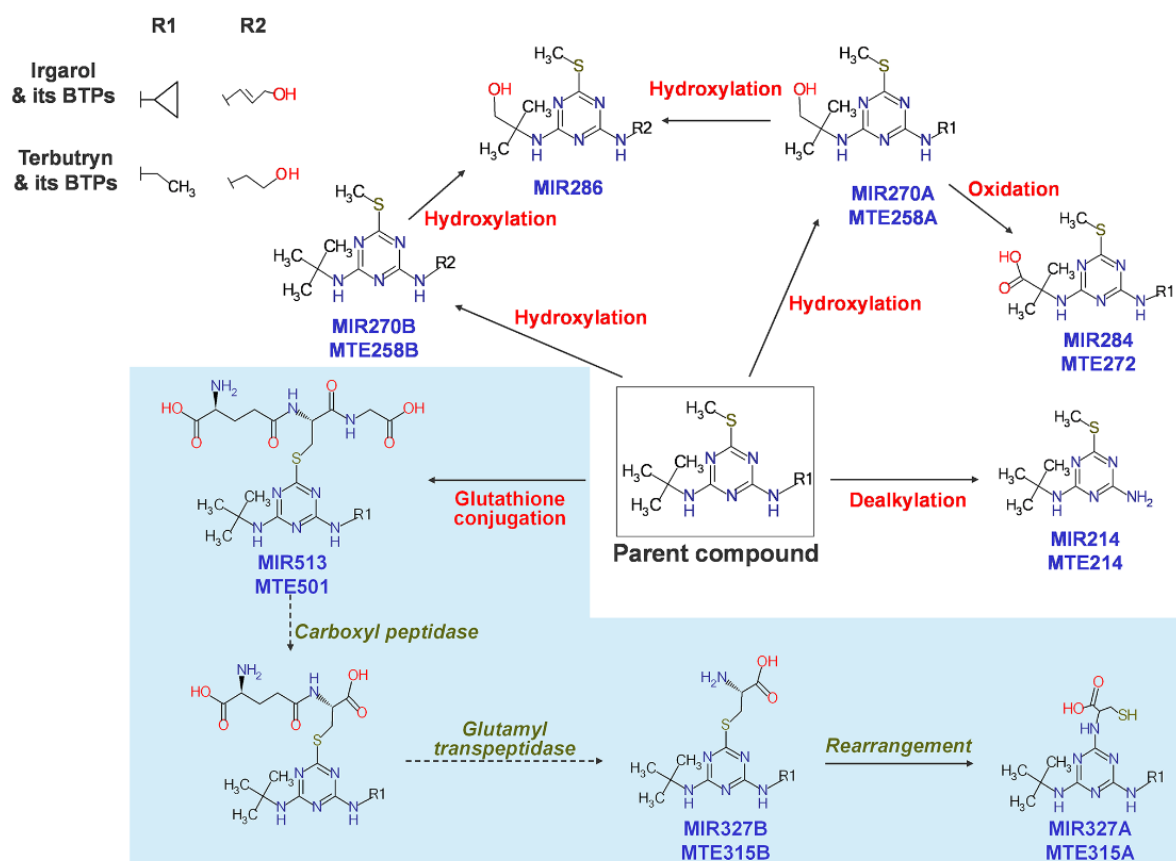


Figure S4: Proposed biotransformation pathways of irgarol and terbutryn in freshwater crustaceans. Note that R2 is the hydroxylated moiety of R1. The sky blue shaded area indicates a pathway including glutathione conjugation followed by subsequent reactions to form cysteine conjugates, reported for the first time in the test organisms.

Figure and caption taken from Jeon et al. (2013). MTE equals the here used shortcut TER_M.

SI A4: Histological staining

The staining protocol is provided in Table S9.

Table S9: Protocol for the HE staining.

Step	Solution	Time
1.	Post fixing in 100% cold EtOH (-20°C)	2 min
2.	Rinse in aqua bidest.	3 min
3.	Hematoxylin (1st staining)	2 min
4.	Wash in running tap water (alkaline)	2 min
5.	1% Eosin (2nd staining)	5 min
6.	Rinse in aqua bidest.	5 min
7.	EtOH 90%	2 min
8.	EtOH 100%	2 min
9.	Rotihistol:EtOH 1:1	2 min
10.	Rotihistol Drying	2 min
11.	Covered with HISTOKitt (ROTH) and glass cover	

SI A5: Medium concentrations

The nominal and measured exposure concentrations of the uptake experiment are presented in Table S10.

Table S10: Exposure concentrations of the uptake experiment. Values were rounded to the significant digits. The deviation of the average concentration from the nominal concentration is provided in the last column. Concentrations can be transformed into molar concentrations by using the molecular weight provided in Table S1.

Compound	Nominal [$\mu\text{g L}^{-1}$]	Start [$\mu\text{g L}^{-1}$]	End [$\mu\text{g L}^{-1}$]	Average [$\mu\text{g L}^{-1}$]	SD [$\mu\text{g L}^{-1}$]	Deviation [%]
Carbamazepine	2200	2290	2200	2250	61	2
Citalopram	800	800	840	820	31	2
Cyprodinil	350	350	330	340	11	-3
Efavirenz	100	92	97	94	4	-6
Fluopyram	500	530	540	540	9	7
Terbutryn	1000	970	970	970	1	-3

SI A6: Bioconcentration potential across different studies

A comparison of bioconcentration factors after 24 h of exposure for the present study and Rath et al. (2023) that applied $50 \mu\text{g L}^{-1}$ for all compounds in a mixture of 12 polar organic contaminants is presented in Figure S5. Please note that no steady state conditions were confirmed and some of the compounds (i.e., citalopram and efavirenz) may not have reached steady state within 24 h.

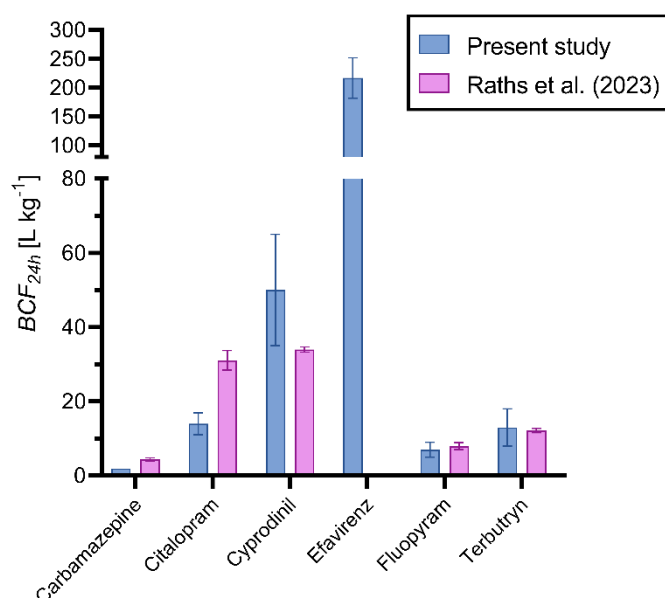


Figure S5: BCF_{24h} across two studies with different exposure mixtures and concentrations.

SI A7: Tissue concentrations

Total tissue concentrations in gammarid tissue not presented in the main manuscript are provided in Figure S6. Absolute concentrations are provided in SI B.

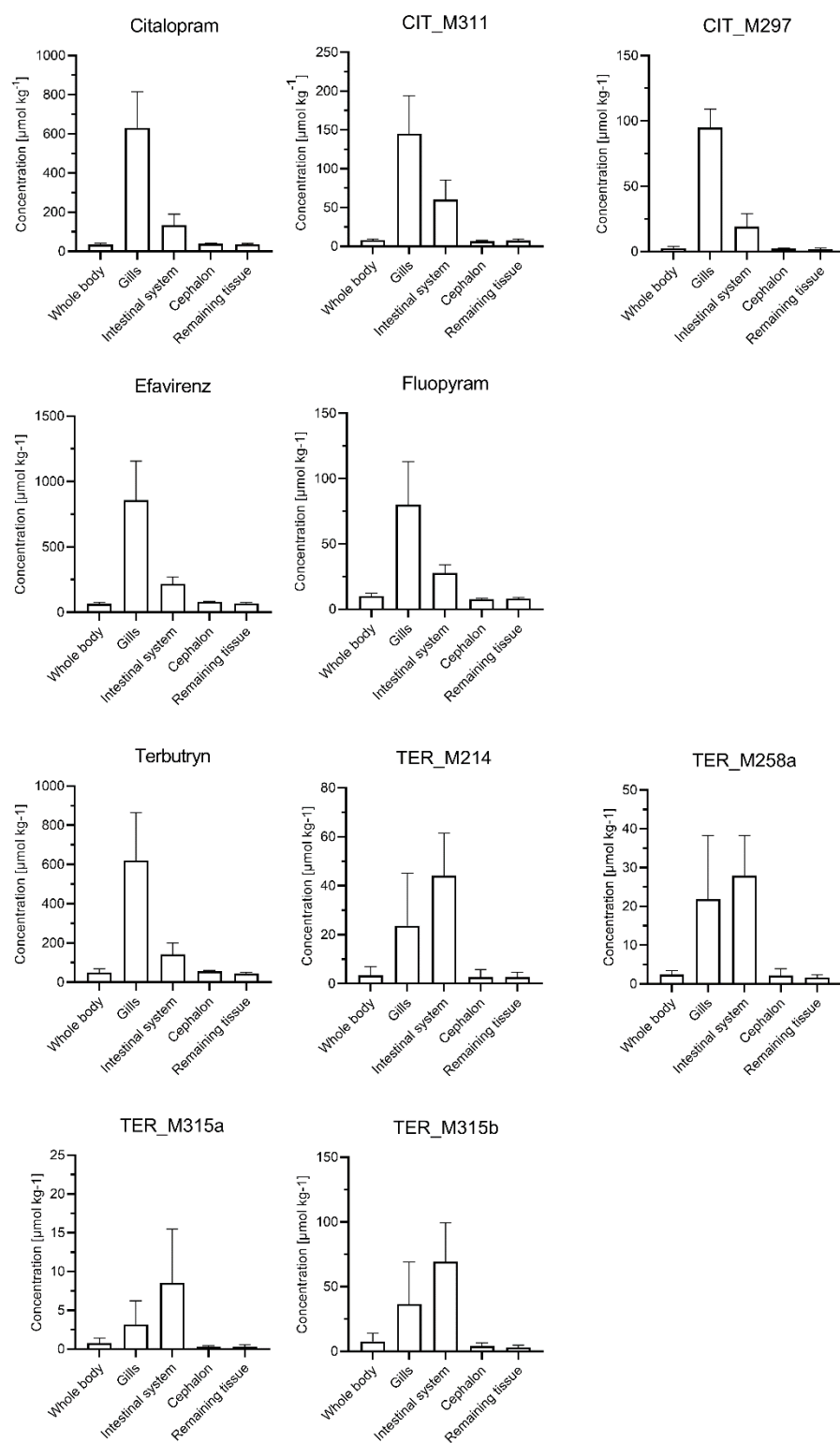


Figure S6: Supplemental graphics of contaminant concentrations in the dissected compartments of gammarids. Whole body = tissue concentration from whole body homogenate extracts. Underlying data are provided in SI B1. Please note the different y-axis scales.

SI A8: Biotransformation ratio across different compartments

The ratio of BTP and parent concentrations in the analyzed compartments is presented in Figure S7. The BTP ratio was highest in the intestine for most of the compounds (except for CMZ_M253 and CIT_M297) and showed little difference between the other compartments.

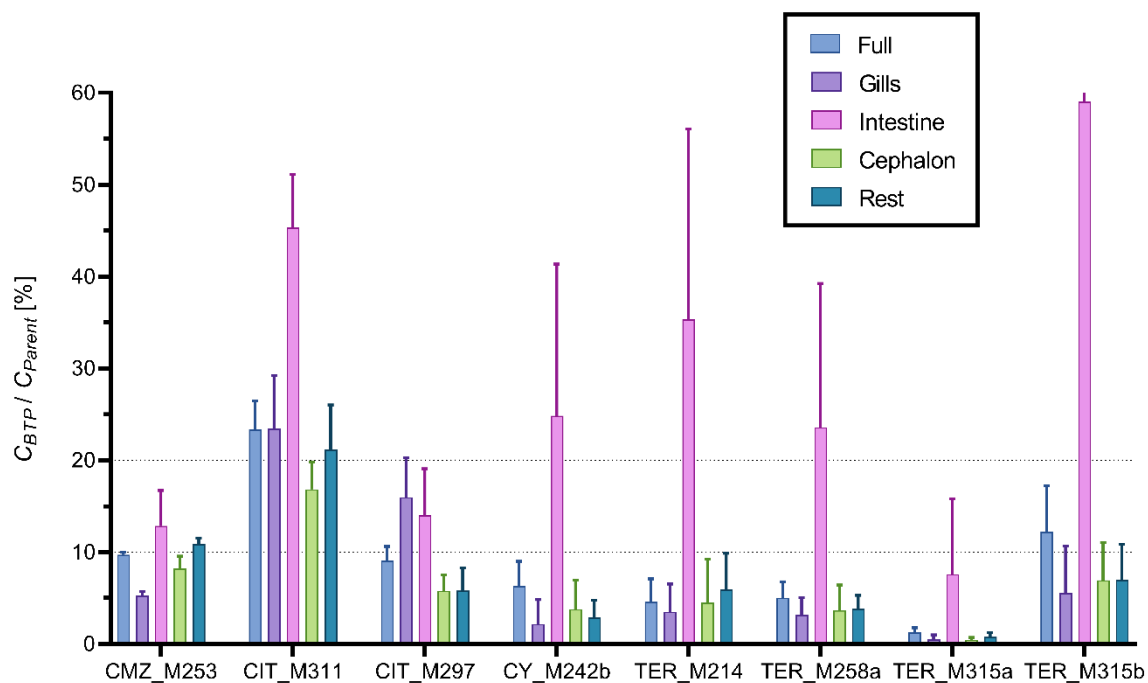


Figure S7: Ratio of the BTP (C_{BTP}) and parent (C_{parent}) concentrations in the analyzed compartments. The ratio was calculated on a molar basis and is presented as percentage.

SI A9: MSI - Supplementary images and replicates

Supplementary images of biomarkers (Fu et al., 2021), parents and BTPs of which only a representative MS-image was presented in the main manuscript (Figure 4) are provided in Figure S8. Additional replicates are provided in Figure S10 to S13.

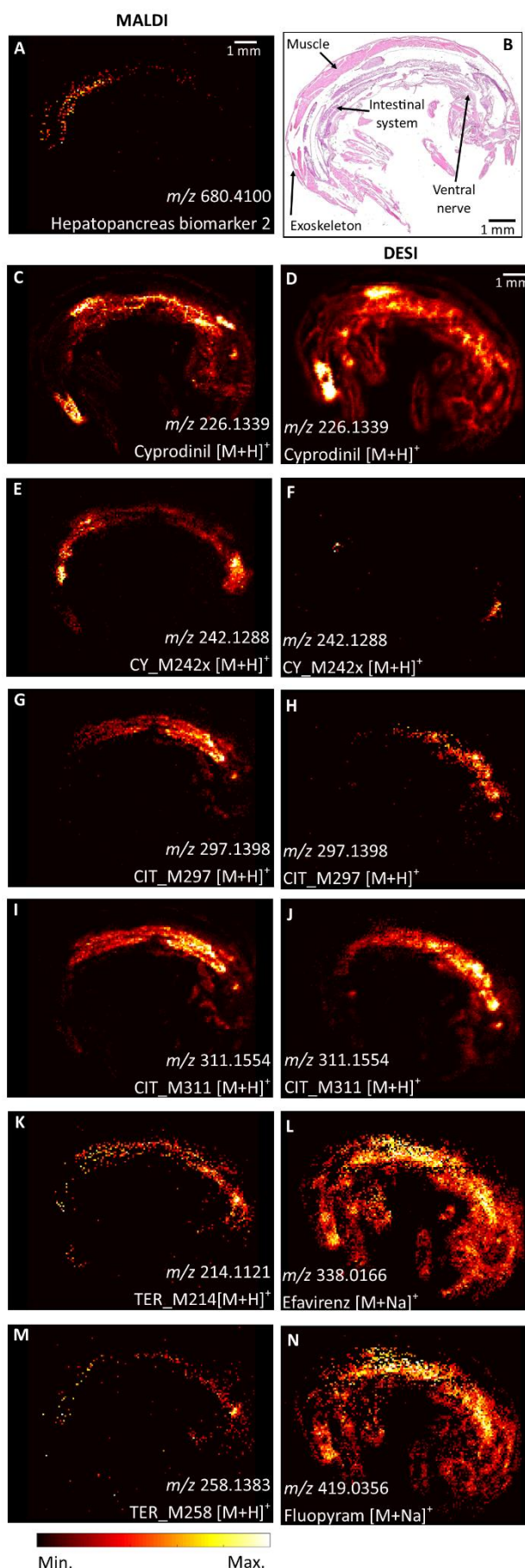


Figure S8: Supplemental MALDI-HRMS (left column) and DESI-HRMS (right column) images for Figure 4 (replicate 1/3, main manuscript). (A) Hepatopancreas biomarker 2. (B) Stained sagittal cryosection. (C + D) Cyprodinil. (E + F) Hydroxylation BTPs of cyprodinil with similar m/z . (G – J) BTPs of citalopram. (K + M) Additional BTPs of Terbutryn, only in MALDI due to mass interferences in DESI (see SI A10). (L + N) Efavirenz and fluopyram only detected in DESI, presented as sodium adducts. The pixel size is 60 μ m.

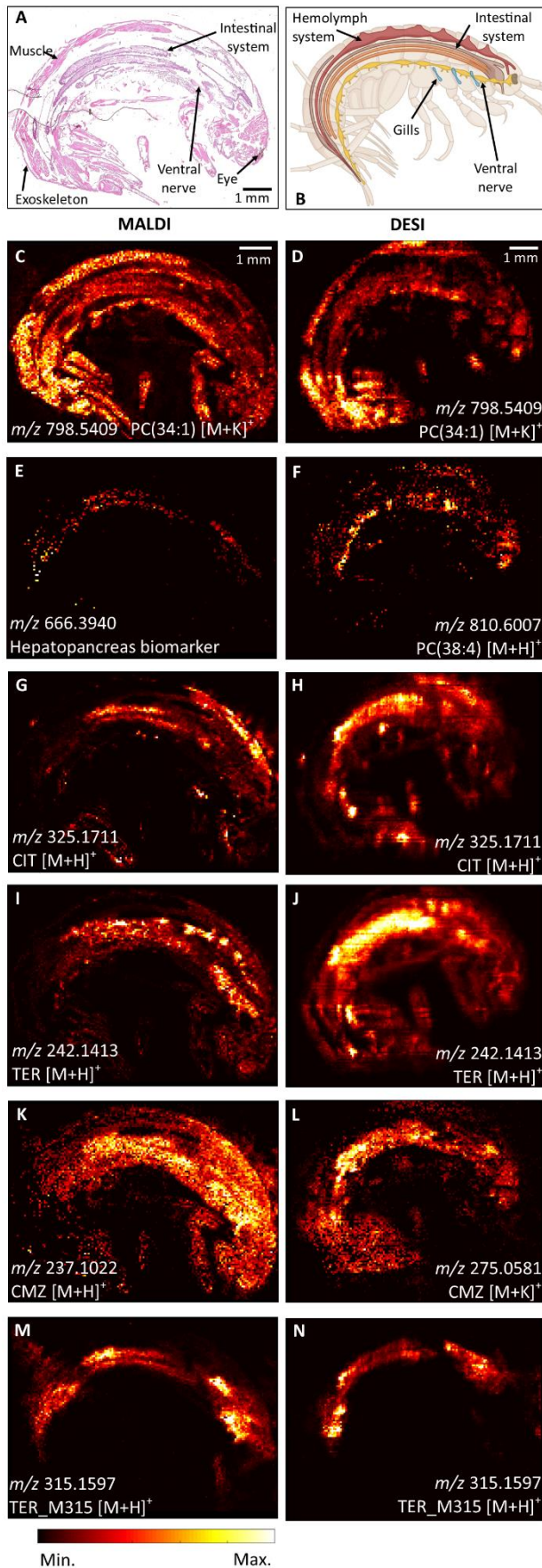


Figure S9: Replicate 2/3, part 1/2. (A) Stained sagittal cryosection. (B) Illustration of different organ compartments in *G. pulex*. Images from MALDI-HRMS on the left and DESI-HRMS on the right side. (C + D) Phosphatidylcholine PC(34:1) for orientation in the MS-images. (E) m/z 666.3940 = biomarker for the hepatopancreas (analogous image for m/z 680.4100) (T. Fu et al., 2021), (F) PC(38:4) as biomarker for the ventral nerve (analogous image to the same mass in MALDI). (G + H) CIT = citalopram, (I + J) TER = terbutryn (analogous image to cyprodinil), (K + L) CMZ = carbamazepine (analogous images for fluopyram and efavirenz [M+Na]⁺), (M + N) TER_M315 (no distinction between a and b possible in MSI) representative for all detected BTPs. The pixel size is 60 μ m.

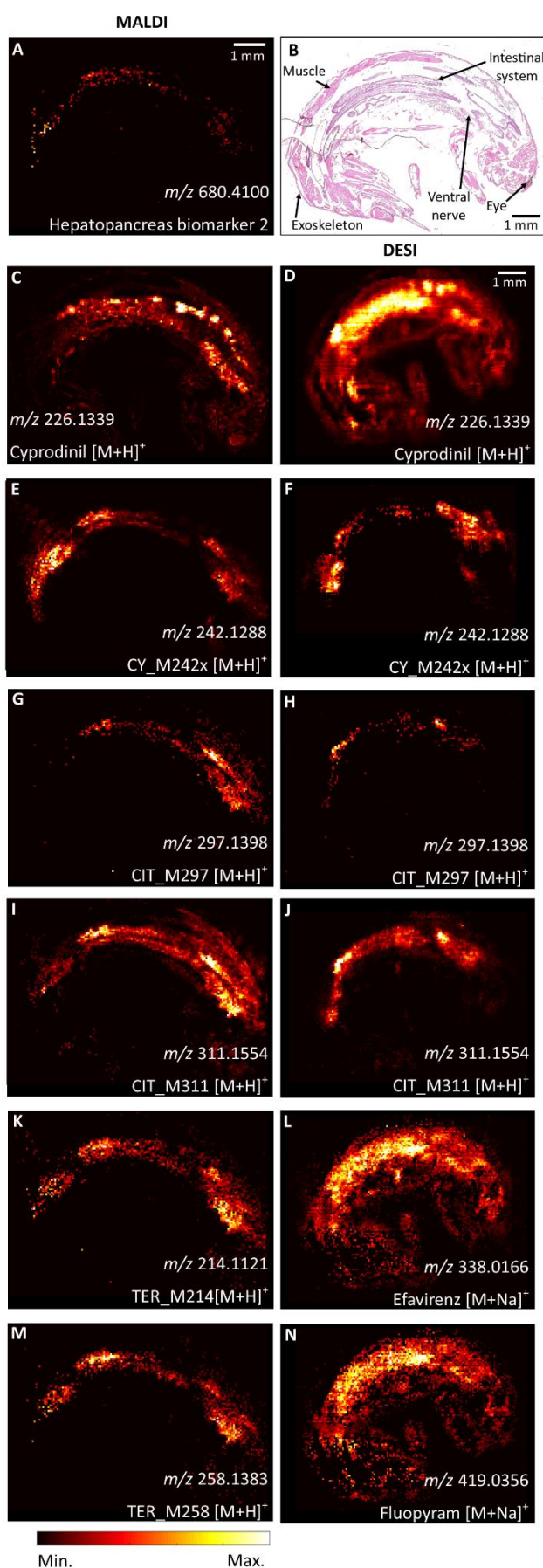


Figure S10: Replicate 2/3, part 2/2. Supplemental MALDI (left column) and DESI (right column) images for Figure S10. (A) Hepatopancreas biomarker 2. (B) Stained sagittal cryosection. (C + D) Cyprodinil. (E + F) Hydroxylation BTPs of cyprodinil with similar m/z . (G – J) BTPs of citalopram. (K + M) Additional BTPs of Terbutryn, only in MALDI due to mass interferences in DESI (see SI A10). (L + N) Efavirenz and fluopyram only detected in DESI, presented as sodium adducts. The pixel size is 60 μm .

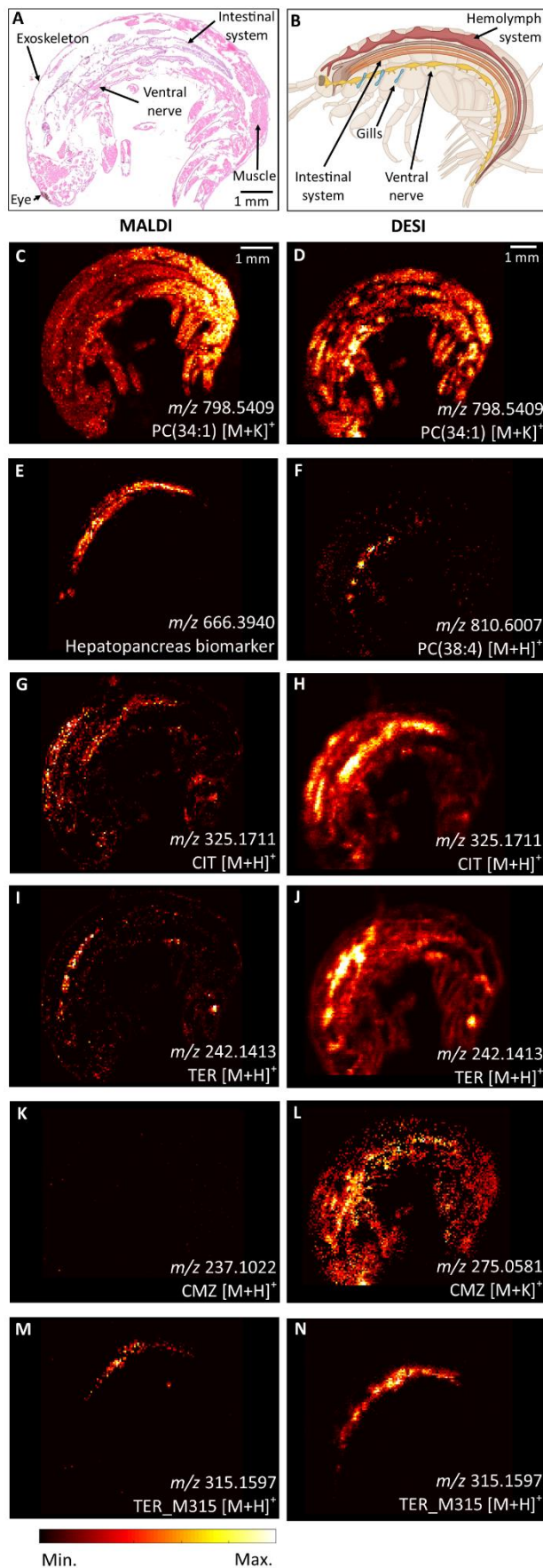


Figure S11: Replicate 3/3, part 1/2. (A) Stained sagittal cryosection. (B) Illustration of different organ compartments in *G. pulex*. Images from MALDI-HRMS on the left and DESI-HRMS on the right side. (C + D) Phosphatidylcholine PC(34:1) for orientation in the MS-images. (E) m/z 666.3940 = biomarker for the hepatopancreas (analogous image for m/z 680.4100) (T. Fu et al., 2021), (F) PC(38:4) as biomarker for the ventral nerve (analogous image to the same mass in MALDI). (G + H) CIT = citalopram, (I + J) TER = terbutryn (analogous image to cyprodinil), (K + L) CMZ = carbamazepine (analogous images for fluopyram and efavirenz [M+Na]⁺), (M + N) TER_M315 (no distinction between a and b possible in MSI) representative for all detected BTPs. The pixel size is 60 μ m.

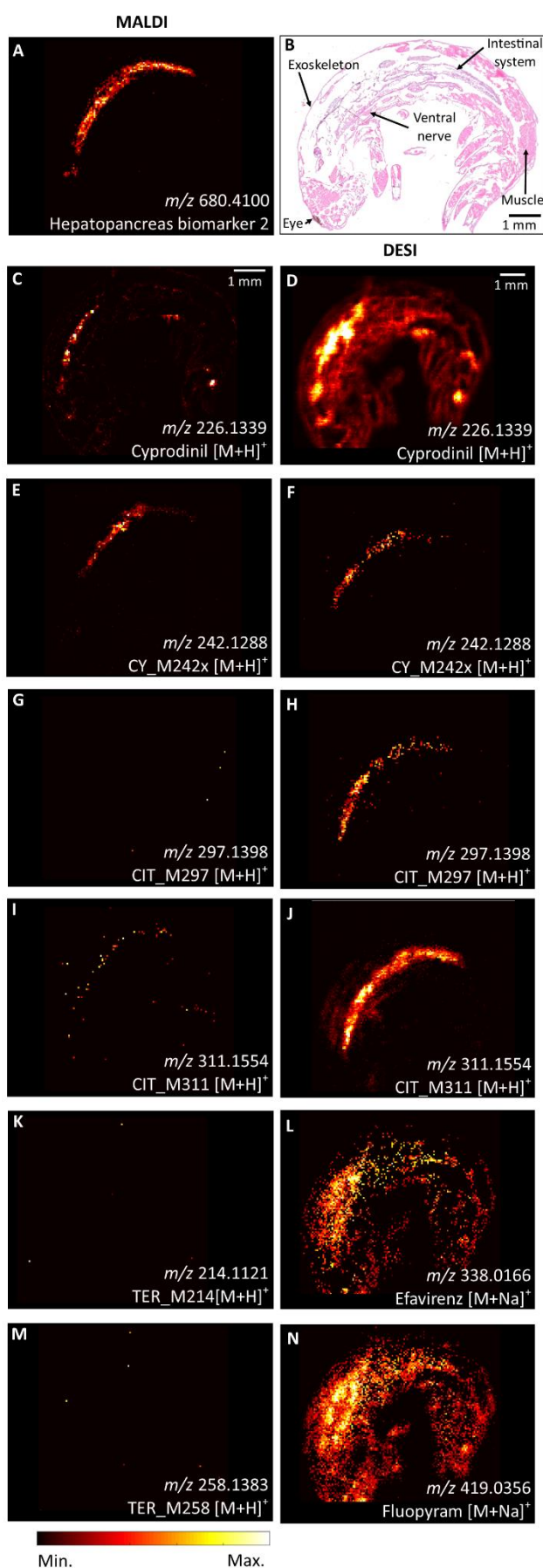


Figure S12: Replicate 3/3, part 2/2. Supplemental MALDI (left column) and DESI (right column) images for Figure S12. (A) Hepatopancreas biomarker 2. (B) Stained sagittal cryosection. (C + D) Cyprodinil. (E + F) Hydroxylation BTPs of cyprodinil with similar m/z . (G – J) BTPs of citalopram (not detected in MALDI for this replicate) (K + M) Additional BTPs of Terbutryn, only in MALDI due to mass interferences in DESI (see SI A10) (not detected in MALDI for this replicate). (L + N) Efavirenz and fluopyram only detected in DESI, presented as sodium adducts. The pixel size is 60 μm .

SI A10: MSI - Mass interferences

The interference of background masses with the detection of TER_M214 and TER_M258^b is presented in Figure S13. The contamination mass was detected all over the analyzed sample of exposed and control sample, but with higher intensities in the intestinal system of exposed gammarids and much lower intensities or absent on the gammarid tissue of the controls. The same pattern persisted for sodium and potassium adducts or a lowered m/z tolerance of $\pm <1$ ppm.

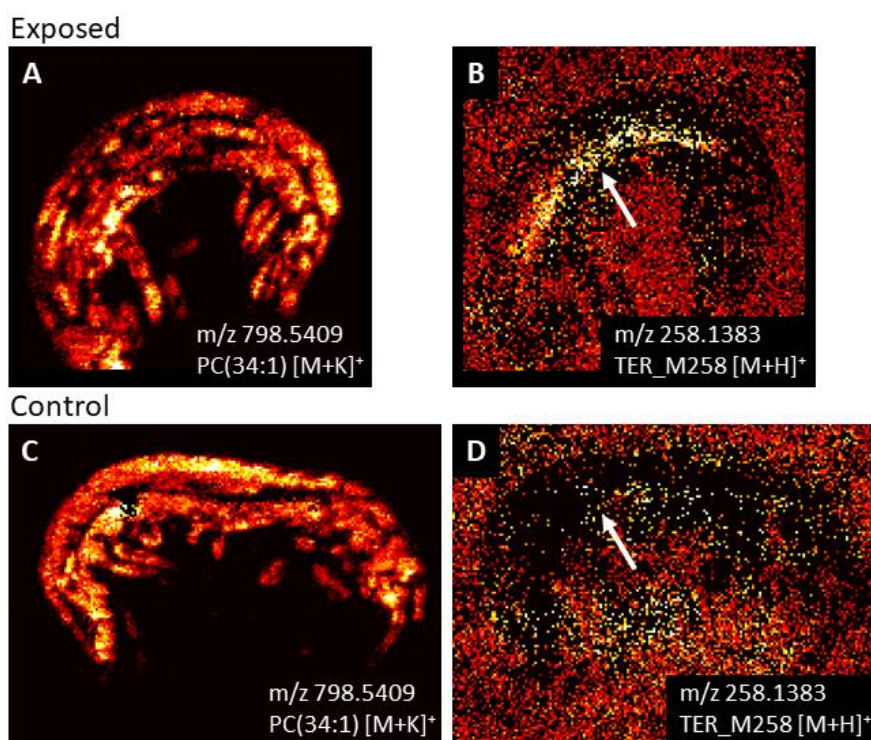


Figure S13: Representative illustration of the mass interferences observed for the BTPs TER_M214 and TER_M258^b in DESI. (A + C) PC(34:1) for orientation in the exposed and control sample, respectively. (B+D) m/z 258.1383 which is the expected [M+H]⁺ for TER_M258. The white arrow indicates the presence of the BTP masses in the intestinal system of exposed gammarids, but absence in the controls.

References

- Ashauer, R., Hintermeister, A., Potthoff, E., Escher, B.I., 2011. Acute toxicity of organic chemicals to *Gammarus pulex* correlates with sensitivity of *Daphnia magna* across most modes of action. *Aquat Toxicol* 103, 38–45. <https://doi.org/10.1016/j.aquatox.2011.02.002>
- Christensen, A.M., Faaborg-Andersen, S., Ingerslev, F., Baun, A., 2007. Mixture and single-substance toxicity of selective serotonin reuptake inhibitors toward algae and crustaceans. *Environ. Toxicol. Chem.* 26, 85–91. <https://doi.org/10.1897/06-219r.1>
- Fu, T., Knittelfelder, O., Geffard, O., Clément, Y., Testet, E., Elie, N., Touboul, D., Abbaci, K., Shevchenko, A., Lemoine, J., Chaumot, A., Salvador, A., Degli-Esposti, D., Ayciriex, S., 2021. Shotgun lipidomics and mass spectrometry imaging unveil diversity and dynamics in *Gammarus fossarum* lipid composition. *iScience* 24, 102115. <https://doi.org/10.1016/j.isci.2021.102115>
- Heye, K., Wiebusch, J., Becker, J., Rongstock, L., Bröder, K., Wick, A., Schulte-Oehlmann, U., Oehlmann, J., 2019. Ecotoxicological characterization of the antiepileptic drug carbamazepine using eight aquatic species: baseline study for future higher tier tests. *J. Environ. Sci. Health Part A* 54, 441–451. <https://doi.org/10.1080/10934529.2018.1562819>
- Huntscha, S., Singer, H.P., McArdell, C.S., Frank, C.E., Hollender, J., 2012. Multiresidue analysis of 88 polar organic micropollutants in ground, surface and wastewater using online mixed-bed multilayer solid-phase extraction coupled to high performance liquid chromatography–tandem mass spectrometry. *J. Chromatogr. A* 1268, 74–83. <https://doi.org/10.1016/j.chroma.2012.10.032>
- Jeon, J., Hollender, J., 2019. In vitro biotransformation of pharmaceuticals and pesticides by trout liver S9 in the presence and absence of carbamazepine. *Ecotoxicol. Environ. Saf.* 183, 109513. <https://doi.org/10.1016/j.ecoenv.2019.109513>
- Jeon, J., Kurth, D., Hollender, J., 2013. Biotransformation pathways of biocides and pharmaceuticals in freshwater crustaceans based on structure elucidation of metabolites using high resolution mass spectrometry. *Chem Res Toxicol* 26, 313–24. <https://doi.org/10.1021/tx300457f>
- Kiefer, K., Müller, A., Singer, H., Hollender, J., 2019. New relevant pesticide transformation products in groundwater detected using target and suspect screening for agricultural and urban micropollutants with LC-HRMS. *Water Res.* 165, 114972. <https://doi.org/10.1016/j.watres.2019.114972>
- Kosfeld, V., Fu, Q., Ebersbach, I., Esser, D., Schauerte, A., Bischof, I., Hollender, J., Schlechtriem, C., 2020. Comparison of Alternative Methods for Bioaccumulation Assessment: Scope and Limitations of In Vitro Depletion Assays with Rainbow Trout and Bioconcentration Tests in the Freshwater Amphipod *Hyaella azteca*. *Environ. Toxicol. Chem.* 39, 1813–1825. <https://doi.org/10.1002/etc.4791>
- Li, C., Yuan, S., Xie, Y., Guo, Y., Cheng, Y., Yu, H., Qian, H., Yao, W., 2021. Transformation of fluopyram during enzymatic hydrolysis of apple and its effect on polygalacturonase and apple juice yield. *Food Chem.* 357, 129842. <https://doi.org/10.1016/j.foodchem.2021.129842>
- Mahaye, N., Musee, N., 2022. Effects of Two Antiretroviral Drugs on the Crustacean *Daphnia magna* in River Water. *Toxics* 10, 423. <https://doi.org/10.3390/toxics10080423>
- Mutlib, A.E., Gerson, R.J., Meunier, P.C., Haley, P.J., Chen, H., Gan, L.S., Davies, M.H., Gemzik, B., Christ, D.D., Krahn, D.F., Markwalder, J.A., Seitz, S.P., Robertson, R.T., Miwa, G.T., 2000. The Species-Dependent Metabolism of Efavirenz Produces a Nephrotoxic Glutathione Conjugate in Rats. *Toxicol. Appl. Pharmacol.* 169, 102–113. <https://doi.org/10.1006/taap.2000.9055>
- Raths, J., Švara, V., Lauper, B., Fu, Q., Hollender, J., 2023. Speed it up: How temperature drives toxicokinetics of organic contaminants in freshwater amphipods. *Glob. Change Biol.* 29, 1390–1406. <https://doi.org/10.1111/gcb.16542>
- Richter, S., Nagel, R., 2007. Bioconcentration, biomagnification and metabolism of ¹⁴C-terbutryn and ¹⁴C-benzo[a]pyrene in *Gammarus fossarum* and *Asellus aquaticus*. *Chemosphere* 66, 603–610. <https://doi.org/10.1016/j.chemosphere.2006.08.002>

- Sangkuhl, K., Klein, T.E., Altman, R.B., 2011. PharmGKB summary: citalopram pharmacokinetics pathway. *Pharmacogenet. Genomics* 21, 769–772. <https://doi.org/10.1097/FPC.0b013e328346063f>
- Sapp, M., Ertunç, T., Bringmann, I., Schäffer, A., Schmidt, B., 2004. Characterization of the bound residues of the fungicide cyprodinil formed in plant cell suspension cultures of wheat. *Pest Manag. Sci.* 60, 65–74. <https://doi.org/10.1002/ps.787>
- Schymanski, E.L., Jeon, J., Gulde, R., Fenner, K., Ruff, M., Singer, H.P., Hollender, J., 2014. Identifying small molecules via high resolution mass spectrometry: communicating confidence. *Env. Sci Technol* 48, 2097–8. <https://doi.org/10.1021/es5002105>
- Vargas-Pérez, M., Egea González, F.J., Garrido Frenich, A., 2020. Dissipation and residue determination of fluopyram and its metabolites in greenhouse crops. *J. Sci. Food Agric.* 100, 4826–4833. <https://doi.org/10.1002/jsfa.10542>